Broadband identification of battery electrical impedance for HEV

Rouba Al-Nazer, Viviane Cattin, Maxime Montaru, Pierre Granjon

BROADBAND IDENTIFICATION OF BATTERY ELECTRICAL IMPEDANCE FOR HEV

R. Al-Nazer, V. Cattin, M. Montaru – CEA LETI/LITEN; P. Granjon – GIPSA-Lab;

Abstract — In recent years, Li-ion batteries have been proposed as an essential element for hybrid electrical vehicles (HEV) and electrical vehicles (EV). In such applications, the most possible accurate estimation of the battery states is needed to optimize its operation. Accordingly, battery electrical impedance is known to be able to provide useful states information. Though that electrical impedance spectroscopy has firmly established itself as one of the most informative investigation method especially because of its accuracy, it cannot be easily implemented in embedded systems. In this paper, broadband excitation signals, frequently used in system identification applications, are proposed to perform impedance measurements on a battery cell. Moreover, spectral coherence is an advanced parameter estimated in order to determine the frequency bands where the transfer function of the system is accurately identified. We propose in this study to test and compare the identification performances of such signals for the broadband monitoring of a battery.

Keywords— battery impedance, spectroscopy, broadband signals, Li-ion battery, coherence, identification.

I. INTRODUCTION

Batteries are an integral part and critical backup system of EV and HEV. Li-ion battery technology is believed to be the most attractive for these applications. It ensures higher power and energy densities, long cycle life, low cost of raw materials and superior safety characteristics [1][2]. In order to ensure safety in vehicles and improve the use of batteries, a Battery Management System (BMS) is involved [3]. It should provide an efficient way to monitor battery performances and assessment of its condition in order to increase the reliability of EV and HEV systems. Several studies [4][5][6] point out the usefulness of cell impedance measurements. For this reason, electrochemical impedance spectroscopy (EIS) [7][8] is frequently used to better investigate the states of a battery. Electrochemical impedance spectroscopy can be performed either in a galvanostatic or in a potentiostatic mode. Following the first approach, a small AC current flows through the storage device under investigation and its AC voltage response is measured. The electrical impedance is estimated from the single frequency AC current superimposed a DC current (charging or discharging and used to define the overall working point of the cell) and the measured AC voltage response [9][10][11]. Though its accuracy, an important drawback appeals research to seek for new ways of operating. Indeed, EIS is still a laboratory technique that cannot be easily implemented in embedded systems. Accordingly, broadband impedance identification using different types of excitation pattern is proposed. The concept consists in measuring the system response at multiple frequencies at the same time.

This paper focuses on the test of these broadband excitation signals and the comparison of their identification performances for the estimation of battery electrical impedance. After a brief review of non-parametric broadband identification basics for linear and time-invariant systems, the method is applied

using simulated data. Spectral coherence is computed to select the frequency band where the system deals with LTI hypothesis. Finally, experimental results that validate the relevance of this approach are presented.

II. NON PARAMETRIC IDENTIFICATION THEORY

A linear and time invariant (LTI) single input single output (SI/SO) system $\mathcal{H}$ is completely characterized by its impulse response $h[n]$ or its frequency response function $H(\lambda)$, which are related by a Fourier transform:

$$H(\lambda) = \sum_{n=-\infty}^{+\infty} h[n] e^{-j2\pi\lambda n} \qquad (1)$$

In this equation, $j = \sqrt{-1}$ and $\lambda \in \left]-\frac{1}{2};\frac{1}{2}\right]$ is the normalized frequency, leading to the frequency f in Hertz when multiplied by the sampling frequency.

Non-parametric identification of LTI systems aims to estimate the frequency response function $H(\lambda)$ from input $x[n]$ and noisy output measurements $z[n]$ (Figure 1) without the use of any model.

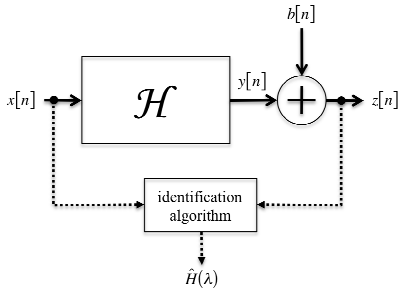

Figure 1: Non-parametric identification of a LTI system $\mathcal{H}$ in the frequency domain.

The unknown additive measurement noise $b[n]$ is supposed uncorrelated with $x[n]$ and therefore with the unnoisy output $y[n]$. Thanks to this last assumption, one can write:

$$S_{zx}(\lambda) = S_{yx}(\lambda) = H(\lambda) S_{xx}(\lambda). \qquad (2)$$

Therefore, on the frequency bands where the input PSD $S_{xx}(\lambda) \neq 0$, the unknown frequency response function $H(\lambda)$ can be calculated through:

$$H(\lambda) = \frac{S_{zx}(\lambda)}{S_{xx}(\lambda)} \text{ if } S_{xx}(\lambda) \neq 0. \qquad (3)$$

This finally leads to the frequency domain identification of the unknown system $\mathcal{H}$. Eq. (3) clearly shows that it is advantageous to use broadband input signals $x[n]$ since they allow the computation of $H(\lambda)$ on a wide frequency band as a whole.

An essential quantity in such a method is the spectral coherence between measured signals $x[n]$ and $z[n]$ [10][11]:

$$\left|c_{zx}(\lambda)\right|^2 = \frac{\left|S_{zx}(\lambda)\right|^2}{S_{xx}(\lambda)S_{zz}(\lambda)}. \qquad (4)$$

This statistical quantity is bounded by 0 and 1, and measures the linear dependency or correlation between $x[n]$ and $z[n]$ at each frequency λ [12][13] and is used in the following to compute confidence limits for different spectral estimators.

The PSD and CPSD used in Eq. (3) and (4) can be easily estimated through the well-known Welch modified periodogram [13]. In this method, measured signals are split-up into L data segments of length N and as an example, the corresponding estimator of the CPSD between $x[n]$ and $z[n]$ is given by:

$$\hat{S}_{zx}(\lambda) = \frac{A}{L}\sum_{k=0}^{L-1} Z_k(\lambda)X_k^*(\lambda), \qquad (5)$$

where:

- A is a normalization factor,
- $Z_k(\lambda)$ (resp. $X_k(\lambda)$) is the Fourier transform of the k^{th} windowed segment of $z[n]$ (resp. $x[n]$),
- * denotes the complex conjugate.

It yields that the spectral coherence $\left|c_{zx}(\lambda)\right|^2$ and the frequency response function $H(\lambda)$ can be estimated by using Eq. (5) in Eq. (3) and (4):

$$\left|\hat{c}_{zx}(\lambda)\right|^2 = \frac{\left|\hat{S}_{zx}(\lambda)\right|^2}{\hat{S}_{xx}(\lambda)\hat{S}_{zz}(\lambda)}, \qquad (6)$$

$$\hat{H}(\lambda) = \frac{\hat{S}_{zx}(\lambda)}{\hat{S}_{xx}(\lambda)} \text{ if } \hat{S}_{xx}(\lambda) \neq 0. \qquad (7)$$

Halliday [14] includes the line $1-(1-95\%)^{1/L-1}$ on the coherence plot as an estimate of the upper 95% confidence limit under the hypothesis of independence. Estimated values of coherence lying below this line can be taken as evidence for the lack of a linear association between input and output. Halliday [14] also used the estimated coherence to compute upper and lower 95% confidence limits for the gain and phase estimates $\hat{G}(\lambda) = \left|\hat{H}(\lambda)\right|$ (Eq. (8)) and $\hat{P}(\lambda) = \arg\left\{\hat{H}(\lambda)\right\}$ (Eq. (9)).

$$\log_{10}\left\{\hat{G}(\lambda)\right\} \pm 1.96\sqrt{\frac{\left(\log_{10}(e)\right)^2}{2L}\frac{1-\left|\hat{c}_{zx}(\lambda)\right|^2}{\left|\hat{c}_{zx}(\lambda)\right|^2}} \qquad (8)$$

$$\hat{P}(\lambda) \pm 1.96\sqrt{\frac{1}{2L}\frac{1-\left|\hat{c}_{zx}(\lambda)\right|^2}{\left|\hat{c}_{zx}(\lambda)\right|^2}} \qquad (9)$$

Finally, Eq. (5) and (7) constitute the "identification algorithm" appearing in Figure 1 and used to estimate the frequency response function $H(\lambda)$ of an unknown LTI system through its input $x[n]$ and

noisy output $z[n]$. Eq. (6), (8) and (9) are used to evaluate the performance of the algorithm by computing 95% confidence limits of the previous estimators.

In what follows, batteries are modelled as electrical LTI systems and are stimulated in galvanostatic mode (the current conrresponds to the input and the voltage response to the output). The corresponding frequency response function is then the electrical impedance of the battery, and this quantity is estimated thanks to the previous set of equations.

III. BROADBAND IDENTIFICATION OF ELECTRICAL IMPEDANCE FOR LI-ION BATTERIES

A. Battery modelling and simulation

Equivalent electrical circuits (EEC) are commonly used to reproduce the battery electrical behavior. They consist on passive (resistors, capacitors, inductors, constant phase elements) and active (voltage and current sources) elements [15]. For electrical engineers, such models are able to characterize electrochemical phenomena, and lead to perform a quick analysis and prediction of the battery behavior in frequency as in time domains [16]. Adapted Randles model (Figure 2) is the EEC adopted in our study. It was developed, used and implemented using Simulink in [14]. It includes the modelling of connectors and electrolyte (R,L), passivation film (R_f // CPE_f), charge transfer (R_{tc}) and double layer phenomena (CPE_{dl}). The open circuit voltage (OCV) is given in a look up table with respect to the current intensity and the battery state of charge. This circuit introduces constant phase elements (CPE) to accurately reflect the behaviour of the battery observed on impedance spectroscopy measurements [17][18].

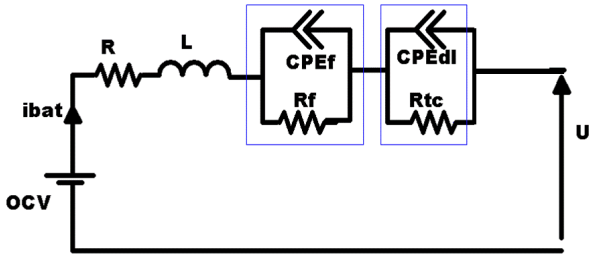

Figure 2. Equivalent electrical circuit (adapted Randles model) of a graphite/$LiFePO_4$ battery

Circuit parameters are function of the state of charge (SOC) and the current intensity. In simulations, theoretical impedance is considered to be the analytical expression of the EEC impedance. In order that the battery meets the requirements of a LTI system described in section II, the whole measurement time should be chosen so that only a little variation of the battery SOC occurs during the identification step.

We focused on the frequency band from 1 to 7 Hz. The simulations are undertaken under the same operating conditions of SOC (60%) and DC current (1A). We consider a time duration of 90 seconds, and the sampling frequency f_s is 700 Hz. These signals are cut into L=10 disjoint segments of length

N=6300 samples. A white Gaussian noise with zero mean and a variance such that the signal to noise ratio (SNR) is 0 dB is added on the output voltage signal to simulate measurement noise. Spectral coherences and electrical impedances are then estimated from this noisy voltage and the excitation signals through Eq. (6) and (7). Estimated electrical impedances are finally compared to the theoretical impedance value in order to evaluate the quality of the broaband identification process.

B. Broadband excitation signals

Broadband identification is valid when the excitation signal shows an almost flat power spectral density in the frequency band of interest. Pseudo random binary sequences (PRBS), swept square (square pattern with a period varying continuously) and a square wave (square pattern with constant period) are broadband signals frequently used in system identification applications [19]. The latter signal is not on itself a broadband signal but can be considered so if its harmonics are in the frequency band of interest. Such signals allow the estimation of the frequency response function of LTI systems, in particular the battery impedance, over a large bandwidth from a single set of measurements. In this work, these broadband signals are introduced as identification patterns that can be used in embedded systems.

Estimate PSDs are computed using Eq. (5) and the same values as those given in section III.A are chosen (L=10, N=6300, f_s=700Hz, T=9s). The resulting PSDs are shown in Figure 3. Under assumption of constant power for the excitation signals, we note that the spectral information is different in levels and frequency bandwidths.

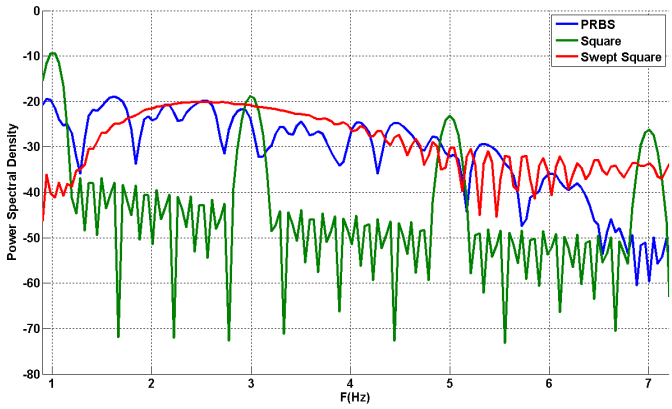

Figure 3. PSD of the three excitation signals.

C. Coherence results

We consider a reasonable measurement noise of SNR=0 dB. Figure 4 shows the coherences estimated with the three excitation signals previously defined, and it can be clearly noticed that the

results are coherent with the PSD. Higher coherence values are obtained within the considered frequency band.

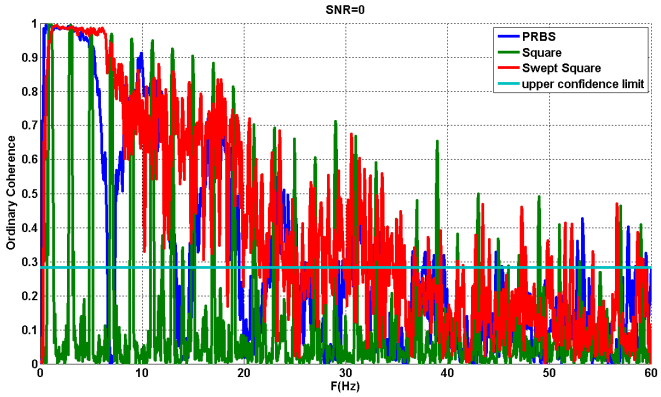

Figure 4. Coherence plots for the three excitation signals with a measurement SNR=0 dB.

D. Confidence limits results

Confidence limits upon the gain and the phase of the estimated impedance quantify the estimation performance reached by this identification method and can be easily computed by using Eq. (8) and (9). In this section, the results concerning the gain factor for PRBS, swept square and square are given as an illustrative example, and they are exclusively represented in the selected frequency band. Phase factor results are very similar.

The different figures of Figure 5 show that the PRBS (Figure 5(a)) has large confidence limits near the upper limit of the band $f_{\max}$, which confirms the coherence results of Figure 4. Moreover, tight confidence limits are observed upon the whole selected frequency band using a swept square (Figure 5(b)). The square wave (Figure 5(c)) provides, as expected, tight confidence limits only around its odd harmonics frequencies. We infer from those results that broadband impedance can be accurately identified with signals composed of square patterns. Such signals are easy to apply to a battery from simple electronic components, for example by using electronic switches.

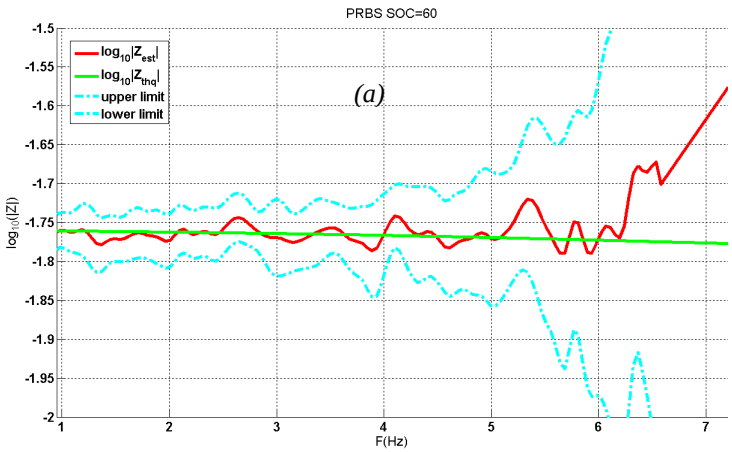

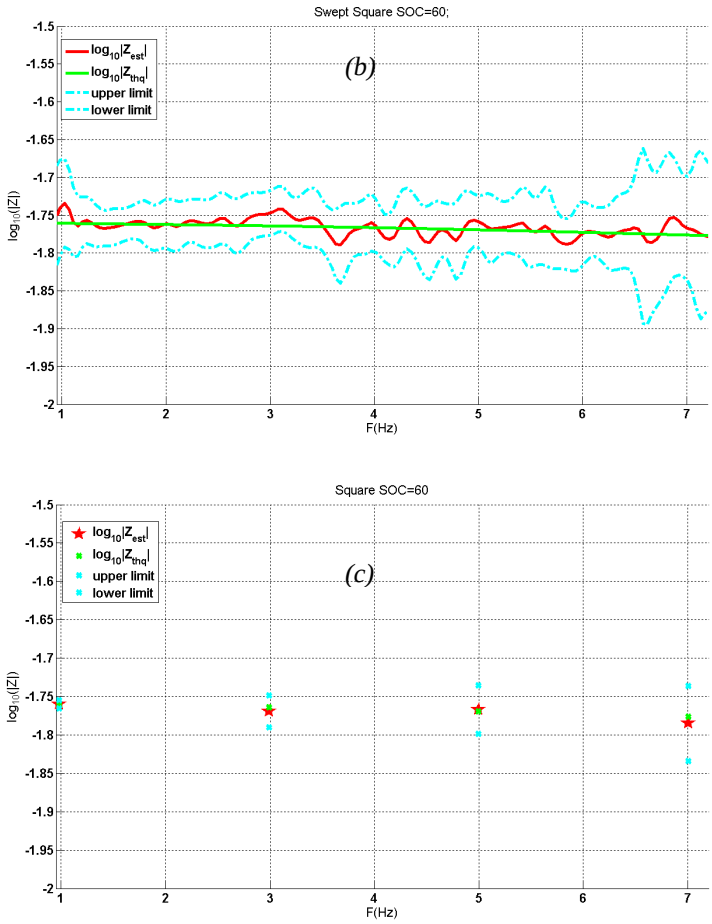

Figure 5. 95% confidence limits results using: (a) PRBS, (b) swept square, (c) square as excitation signals with a measurement SNR=0 dB.

IV. EXPERIMENTAL RESULTS

A. Hardware and implementation

This work was realized on a graphite/LiFePO4 cell with a nominal capacity of 2.3 Ah (ANR26650m1 battery from A123 Systems Company Ltd). Experiments have been carried out at room temperature. As a first step, we consider the same operating conditions that those taken in simulations (SOC of 60% and DC current of 1A, number of blocks L=10, T=9s). We also consider the same frequency band [1Hz – 7Hz] for different SOCs. The goal is to verify if broadband impedance identification can recover the known distortions Nyquist plots with the evolution of the battery SOC. A specific electronic circuit was designed to perform the experiments and to allow application of input current with squared patterns, particularly swept square, PRBS and square.

B. Experimental results

1) PRBS, swept square and square for a frequency band of 1 -7Hz

The broadband signals based on squared patterns are applied to the battery. The corresponding estimated coherences are plotted in Figure 6 (d), (e) and (f) , while Figure 6 (a), (b) and (c) show the

estimated electrical impedance. The coherence is clearly close to 1 all over the specified frequency band for PRBS and swept square signals while it has only strong values at odd harmonics of the square signal as predicted This shows that the battery can be considered as a LTI system under the operating conditions used, and that its electrical impedance will be correctly estimated. As shown by simulations of section III. it can also be noticed that the use of a PRBS current induces a decrease in the coherence near the upper limit frequency $f_{\max}$. Accordingly, the variability of the estimated impedance with the different signals is very small all over the frequency band, unless near the upper frequency for PRBS.

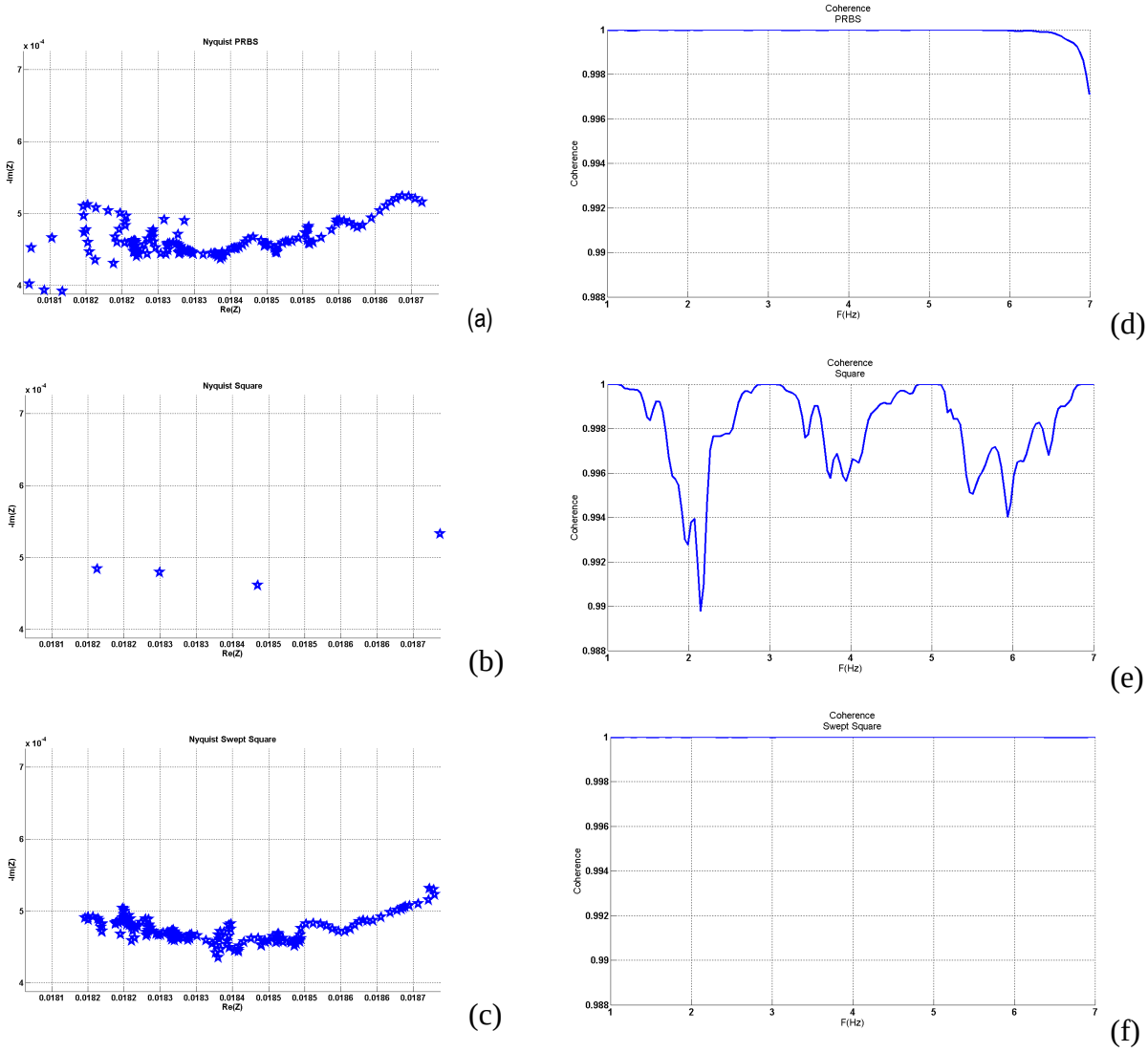

Figure 6. Experimental results: Nyquist plots - (a) PRBS, (b) square, (c) swept square coherence plots - (d) PRBS, (e) square,(f) swept square.

Based on the high coherence values obtained during experiments, this battery can be considered as a LTI system within the chosen frequency band and under the chosen operating conditions. Moreover, confidence limits of impedance estimators are sufficiently small to affirm that the electrical impedance is

accurately identified all over the frequency band, and that the swept square input current leads to better results than the PRBS.

2) ***PRBS for a frequency band of 1 - 7Hz at different SOCs***

Several studies reveal that the SOC distorts the battery electrical impedance at lowest frequencies. In this context, we design a PRBS that can excite the frequency band of [1 - 7] Hz. The choice of PRBS is based on the previous results that showed the strong performances of this excitation signal near the lower limit frequency band. Exciting low frequencies yields that the number of blocks L used for averaging cannot be higher than done previously (because of LTI assumptions). In that case it will be limited to L=10 blocks of duration 9 seconds each. The sampling frequency is unchanged. The battery is stimulated under several SOC (45, 60, 90 %) and for each SOC a broadband identification step is performed.

Figure 7 shows that the PRBS is able to reflect the SOC effect on the battery electrical impedance. With a small time measurement (90 s), this method is thus able to accurately estimate the battery impedance for low frequencies. We can ensure the quality of the estimation thanks to the coherence values which are once again very close to 1 .

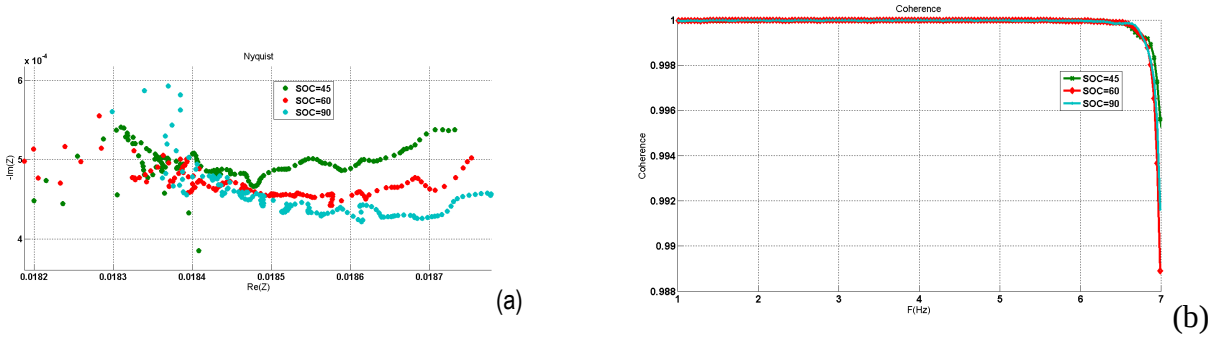

Figure 7. Experimental results with PRBS signal and under several SOCs:- (a) Nyquist plots, (b) coherence plots.

V. CONCLUSION

This paper focuses on the usefulness of broadband excitation signals for the identification of a Li-ion battery electrical impedance. After a review of non-parametric identification theory and advanced parameters such as coherence function and confidence limits, the simulation results ensure that this method can be applied to battery systems. Experimental tests performed at a low frequency band reveal that signals based on square pattern like swept square, PRBS and square lead to correct broadband identification results. They are particularly well suited for electronic implementation. Experimental results also obtained at a low frequency band for different SOCs confirm the possibility to apply PRBS to batteries to monitor their SOC evolution. These results are promising to improve and enhance actual BMS.

The authors thank Marco Ranieri for its contribution to this work.

REFERENCES

[1] Wakihara M. and Yamamoto O., (1998). *Lithium ion batteries: fundamentals and performance*, Wiley-VCH.

[2] Matsuki, K. and Ozawa, K. (2010), *General Concepts, in Lithium Ion Rechargeable Batteries: Materials, Technology, and New Applications* (ed K. Ozawa), Wiley-VCH Verlag GmbH & Co. KGaA, Weinheim, Germany. doi: 10.1002/9783527629022.ch1.

[3] Davide A., (ed) (2010) *Battery management systems for large Lithium-Ion battery packs*. Artech House, Boston – London.

[4] Montaru M. Pelissier S., (2008). *Frequency and temporal identification of a Li-ion Polymer battery model using fractional impedance.* Les rencontres scientifiques de l'IFP - Advances in hybrid powertrains.

[5] Robinson R.S., (1993). *System noise as a signal source for impedance measurements on batteries connected to operating equipment*. Journal of Power Sources,Volume 2, p.365-368.

[6] Kozlowski J.D., (2003). *Electrochemical Cell Prognostics using Online Impedance Measurements and Model-Based Data Fusion Techniques*. Proceedings of the IEE Aerospace conference.Volume 7, p.3257-3270.

[7] Buller S., (2002). *Impedance-Based Simulation Models for Energy Storage Devices in Advanced Automotive Power Systems*, Thesis, Institute for power electronics and electrical drives ISEA, Aachen/Germany.

[8] Barsoukov, E. and Macdonald, J. R. (eds) (2005). *Frontmatter, in Impedance Spectroscopy: Theory, Experiment, and Applications*, Second Edition, John Wiley & Sons, Inc., Hoboken, NJ, USA

[9] P. Carbonini, T. Monetta, D.B. Mitton, F. Bellucci, P. Mastronardi, B. Scatteia,, (1997). *Degradation behaviour of 6013-T6, 2024-T3 alloys and pure aluminium in different aqueous media*, Journal of Applied Electrochemistry, Volume 27, p.1135-1142.

[10] L. Garrigues, N. Pebere, F. Dabosi, (1996). *An investigation of the corrosion inhibition of pure aluminium in neutral and acidicchloride solutions*, Electrochimica Acta, Volume 41, p.1209-1215.

[11] J.C. Uruchurtu, (1991). *Electrochemical investigations of the activation mechanism of aluminium*, Corrosion Volume 47, p. 472-479.

[12] Shin K., Hammond J.K., (Ed) (2008). *Fundamentals of Signal Processing for Sound and Vibration Engineers*. West Sussex PO19 8SQ, England.

[13] Bendat J.S., Piersol A.G. (2010). *Random data: analysis and measurements procedures*. Fourth Edition, John Wiley & Sons, Inc., Hoboken, NJ, USA

[14] Halliday D.M, Rosenberg J.R al (1995). *A framework for the analysis of mixed time series/point process data-theory and application to the study of physiological tremor, single motor unit discharges and electromyograms*. ELSIVIER Science, Volume 64, No. 2/3, p.237-278.

[15] Urbain M., (2009). *Modélisation électrique et énergétique des accumulateurs Lithium-Ion. Estimation en ligne du SOC et SOH*. Thesis, Institut National Polytechnique de Lorraine, France.

[16] Dong K., (2011). *Dynamic Modeling of Li-Ion Batteries Using an Equivalent Electrical Circuit.* Journal of the Electrochemical Society, Volume 158 (3), p.A326-A336.

[17] Oustaloup A., (1995). *La dérivation non entière : Théorie, Synthèse et Applications*, Editions Hermes.

[18] Oustaloup A., (2005). *Représentation et identification par modèle non entier*, Hermès Sciences.

[19] Pintelon R., Schoukens J., (2001). *System identification, a frequency domain approach.* First Edition, IEEE press marketing, Piscataway,NJ (ISBN 0-7803-6000-1).